Wiley
Advances in Materials Science and Engineering
Volume 2024, Article ID 7424560, 14 pages
https://doi.org/10.1155/2024/7424560

WILEY

Research Article

High-Pressure Torsion: A Simulation Approach for Additive Friction Stir Deposition Processes

Dmytro V. Pavlenko,[1] **Daria V. Tkach**,[1] **Yevgen V. Vyshnepolskyi**,[1] **Myroslava O. Schetinina**,[1] **and Oleksandr F. Tarasov**[2]

[1]*Mechanical Engineering Department, Zaporizhzhia Polytechnic National University, Zhukovskogo 64, Zaporizhzhia 60063, Ukraine*
[2]*Computer Information Technologies Department, Donbass State Engineering Academy, Akademichna 72, Kramatorsk 84313, Ukraine*

Correspondence should be addressed to Myroslava O. Schetinina; majtimo11@gmail.com

Received 5 June 2024; Accepted 20 August 2024

Academic Editor: Senthil Kumaran Selvaraj

The technology of manufacturing aluminum alloy workpieces using additive friction stir deposition (AFS-D) has been thoroughly investigated. The ambiguous influence of deformation processing modes on the material density was found. Examination of the microstructure in the central zone of the specimens reveals the absence of microdefects typically associated with workpieces obtained through casting or powder metallurgy methods. It has been observed that the distribution of microhardness is significantly affected by the direction of specimen construction, with approximately a 20% difference in values between the periphery and the central part of the specimen. Specimens produced using the AFS-D method exhibit a homogeneous microstructure characteristic of deformable aluminum alloys. Notably, a uniform distribution of intermetallides on the specimen surface has been identified. This outcome is likely a result of the alloy undergoing recrystallization during the severe plastic deformation process, leading to the formation of an ultradisperse structure. It is important to emphasize that the selection of technological parameters for AFS-D should consider not only the magnitude of pressure and deformation but also the deformation speed.

Keywords: aluminum alloy; friction stir additive manufacturing; high-pressure torsion; homogenization; microhardness; microstructure; severe plastic deformation

1. Introduction

The rapid evolution of additive manufacturing (AM) methods has driven their increasing popularity. AM has burgeoned into a multi-billion-dollar industry, encompassing diverse sectors of human life. AM methods are modern technologies that create a product by applying material layer by layer to the finished part. Among the main advantages of these production methods is a significant reduction in the time and cost of manufacturing a new product, which is crucial in today's world [1].

Aluminum alloys are used in the construction of aircraft engines mainly for stator parts. In this case, the technologies of workpiece production are usually based on various casting methods. Casting stands as an economically viable method for high-volume production. However, as modern aircraft production leans toward developing new products and engaging in small-scale production, the necessity to manufacture expensive and intricate casting tooling significantly inflates both part costs and production timelines.

One of the promising technologies for the production of aluminum alloy airframe parts is based on additive methods. Aluminum products are predominantly generated by selective sintering of aluminum alloy powders using laser or electron beam heating sources. In the aircraft industry, the AM method, which uses aluminum alloy wire instead of

powder, is gaining popularity [2]. The directed energy deposition (DED) method is an AM process in which focused thermal energy (e.g., laser, electron beam, electric arc, or plasma arc) is used to melt wire materials; that is, it occurs with a transition to the liquid phase [3]. The advantage of this method lies both in the production of parts and in carrying out repairs. However, the direct growth method also has a number of disadvantages that significantly limit its application: low accuracy, high heating leading to structural changes, elevated energy consumption, and equipment cost.

These challenges are relevant for the whole range of aircraft structural materials including aluminum alloys. The main problem with silumines, the most prevalent aluminum alloys in aircraft construction, is their relatively low strength and ductility characteristics. As coarse silicon inclusions in the eutectic phase are the main factor in reducing the strength of pre-eutectic silumines, enhancing the dispersibility of silicon crystals emerges as a pivotal goal for improving their properties. For this purpose, methods to influence the structures including severe plastic deformation (SPD), sodium modification, and heat treatment are used.

Studies in the field of improving the quality of aluminum alloys by deformation processing have shown the high efficiency of SPD methods [4]. Thus, it is reasonable to anticipate that the integration of 3D printing techniques for aluminum workpieces, in tandem with SPD, will yield significant enhancements in the quality of the produced workpieces.

In modern conditions, additive technologies find applications across various industries, including medicine, mechanical engineering, and aircraft construction. The most common methods of obtaining products from metals and alloys are selective laser sintering [5] and fusion, as well as electron beam deposition [6]. Despite the numerous evident advantages offered by additive technologies in comparison with traditional methods, these innovative approaches also exhibit certain disadvantages associated with low mechanical properties of the obtained products and the need for further postprocessing [7]. Furthermore, the process of powder melting results in the formation of a cast structure characterized by large grain size, liquations of alloying elements, and noncontinuities. This not only reduces mechanical properties but also leads to an increase in their dispersion. Thus, many methods used in AM of metal and alloy-based products based on melting allow to obtain parts of complex shapes, but do not allow to achieve high structural characteristics due to the transition from liquid to solid phases [8]. Workpieces obtained through these methods entail substantial production costs, as they necessitate specialized equipment for implementation. They also exhibit residual stresses due to the rapid solidification following the melting of metal powders, which compromises the precision of the final products and mandates compulsory heat treatment. Therefore, contemporary industrial production requirements for product properties are not always met by these technologies, underscoring the necessity to explore alternative AM approaches [9, 10].

Additive friction stir deposition (AFS-D) [11–13] is one of the promising methods for producing high-strength products. The application of this technology makes it possible not only to manufacture products from existing metals and alloys but also to create new composite compounds and architectural materials with specified properties [13–15]. The authors of works [7, 16] proposed to use this process to obtain coatings. It was found that this technology offers excellent adhesion to the substrate material and yields a satisfactory coating structure. In [17], the adhesion strength of coatings obtained by AFS-D at different process parameters was evaluated by bending tests. Bending tests revealed the presence of small delaminations without signs of fracture at the interface at the selection of certain parameters of this method, which confirms the need for a wide study of the influence of technological parameters on coating properties.

In a previous study [18], a model for evaluating the structure and mechanical properties of products obtained by this method was developed. To assess the adequacy of the proposed model, an experimental evaluation was carried out. It was found that the grain size and mechanical properties are significantly affected by technological parameters [18–20]. In particular, the average grain sizes of different layers depend on the temperature of the stirring and restirring processes. An increase in layer thickness can result in a decrease in the reheating and stirring temperature, a reduction in the average grain size, and an increase in the stiffness within the stirring zone [18]. The peculiarities of AFS-D technology make it possible to produce products from light alloys with high mechanical properties. In particular, products from magnesium- and aluminum-based alloys produced by this method have hardness 15%–20% higher compared to those manufactured using conventional technology [21], with mechanical properties remaining consistent. The authors of [22] point out that an important factor determining the quality of deposition is the process temperature. In addition to technological parameters, the process temperature is significantly influenced by the material and thickness of the substrate.

As mentioned above, the properties of products are significantly influenced by technological parameters, and the appropriate selection of these parameters facilitates the attainment of a submicrocrystalline structure [3]. It is likely that recrystallization processes occur during AFS-D contributing to the formation of a fine-grained equiaxed structure. However, when producing products from aluminum alloys, repeated recrystallization may occur, resulting in a reduction in their mechanical properties [23]. In [24], it is indicated that further heat treatment of aluminum alloy 7055 does not lead to a significant change in mechanical properties, and it is suggested to vary the technological parameters of AFS-D to improve them.

Despite the extensive research conducted on aluminum alloys, which possess relatively low melting points, the literature also contains data demonstrating the successful application of this technology in the friction welding of steels, nickel, and titanium alloys [25, 26]. Consequently, obtaining bulk products from alloys with a higher melting point is possible, but requires a set of studies.

Thus, AM by friction stirring is a promising method for obtaining critical products that require high mechanical properties. The main disadvantage of this method is the

necessity for additional mechanical processing of the product to obtain the specified dimensions. However, advantages such as preservation of structure heredity and in some cases its improvement, absence of alloying element loss, low residual stresses due to lower temperatures during friction stirring, and reduced gas emissions in the process make this method exceptionally promising for product manufacturing.

The AFS-D method provides great opportunities for obtaining products with high mechanical properties, eliminating the need for preliminary structural homogenization of the initial materials. This is because the frictional stirring process can be regarded as the SPD process. Consequently, it becomes imperative to investigate the homogenization processes and the influence of processing modes on the structure and properties of workpieces subjected to SPD. Treatment of bulk workpieces from the point of view of material homogenization research is a time-consuming and resource-consuming process. An alternative option is to conduct studies on small-sized specimens subjected to severe deformation by high-pressure torsion (HPT).

In [27], the authors assume that the deformation pattern in friction stir welding is close to simple shear. Consequently, as AM by friction stirring is actually the development of friction welding process to produce bulk products, specimens obtained by HPT can be used to investigate processes occurring in thin layers during product manufacturing.

At the current stage of AFS-D technology advancement, a large number of technological equipment has been developed to support this process. Thus, works [28–30] describe methods and tools for applying material to surface using frictional heating and compressive loading. However, they do not specify how powder or electrode is fed and pressurized or whether it is possible to supply material consistently or only discontinuously. Study [31] introduces tool and method for producing coatings via friction welding, employing spindle through which material is continuously or intermittently fed. It is proposed to use powder or granules as the material for coating application, which is fed into place by a screw. The speed of the screw and spindle can be set and varied according to the operator's desire. In [32], a layer-forming tool is described, characterized by the design of a simple cylinder with protrusion through the axis of which material in powder form is fed.

At this stage of development, AFS-D technology demonstrates its capability to work with an array of materials, including magnesium, aluminum, copper, high-strength steels, and various composite materials such as aluminum with silicon carbide filler. The process involves the gradual buildup of material by forcibly embedding it into the substrate or previous layer. This method ensures high isotropy and density without actual melting of the metal, thus mitigating issues related to shrinkage and risk of hot cracks. Moreover, this technology facilitates the creation of gradient structures by constructing separate sections from different metals or alloys, as well as applying layers from mixtures of two or more materials. Obviously, the resolution of 3D printing is low, but the emphasis is on productivity and reducing waste in the postprocessing of the resulting workpieces. The first commercial model of a 3D printer using rotary friction welding technology, designated as B8, is capable of building parts up to 915 mm × 305 mm × 305 mm in size. One of the remarkable aspects of this technology is its ability to operate without requiring a vacuum chamber or protective gas environment.

The AFS-D process is based on the core principles of friction stir welding. In friction stir welding, a rotating pin moves between the workpieces intended for joining. As a result of friction, the material of the workpieces is melted and a strong joint is formed. The AFS-D technology is based on the rotation of the tool, forcefully pressed against the substrate. This process induces substantial heating in the contact zone, facilitating the application of the initial layer, and this sequence is repeated as needed. The tools are bars, metal powder, or wire [33]. The main disadvantage of using wire and powder is the impossibility to realize in the plastic deformation zone shear stresses sufficient for structural element fragmentation, as well as to use different materials for different layers. At the same time, the use of bar workpieces necessitates periodic replacement, resulting in the formation of "cold joints." However, in this case, in the plastic deformation zone, conditions are created that allow to provide SPD of the material, contributing to a significant increase in the level of mechanical properties and a decrease in the value of their dissipation.

Literature analysis has shown the promising application of additive technologies based on friction stir welding for the production of machine part workpieces. However, the multitude of existing variants of this technology and the corresponding array of process parameters, compounded by the variety of materials handled, have posed challenges in establishing clear criteria for their selection. Also, the questions concerning the effectiveness of employing AFS-D to produce aluminum workpieces with a high level of mechanical properties and the influence of construction modes on the material structure remain relevant.

The purpose of this study is to evaluate the efficiency of the AFS-D method for aluminum workpieces, as well as to determine the main tasks and research directions for its industrial implementation. To achieve the set goal, the tasks related to physical modeling of the process involving mixing and deformation of metal under pressure; exploration of hardness, structure, and phase composition of deformed specimens; distribution of alloying elements; and investigation of the structure and hardness of workpieces obtained by the AFS-D method were solved. The tasks that must be solved for its industrial implementation were also identified and categorized.

2. Materials and Methods

Specimens made of AlSi10Mg-0403 alloy (Si—9.6%, Mg—0.3%, Fe—0.1%, Mn—0.1%, and the rest—Al) obtained by selective laser sintering of powder mixture on a Concept Laser 3D printer were studied. Deformation of cylindrical-shaped specimens (with a diameter of 10 mm and a height of 1 mm) was carried out by applying pressure of 5 GPa and torsion for five full revolutions at room temperature (Figure 1). The torsional speeds were 0.5 and 1 rpm. Both

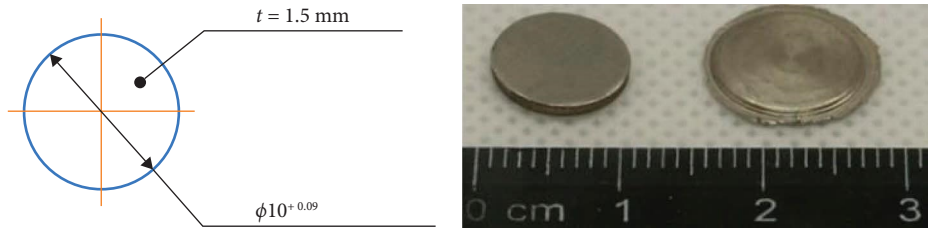

(a) (b)

Figure 1: Sketch (a) and general view of specimens in the initial state and after HPT treatment (b).

specimens experienced an equivalent strain of approximately 60. The specimen density was determined by hydrostatic weighing, which was carried out on electronic analytical scales of XA 310/X type.

Metallographic studies, to identify the features of the specimen structure, were performed. The structure was studied using a Zeiss Axio Observer optical microscope.

Microhardness distribution studies across the cross section of the specimens were performed on the unetched grinds after pretreatment with fine abrasive sandpaper (Figure 2). To exclude the appearance of secondary hardening and pore rubbing, grinding was carried out under constant load on a MECATECH 234 grinding and polishing machine equipped with an automatic specimen holder.

Microhardness measurements were conducted using an HVA-1 microhardness tester equipped with an automated loading device, ensuring a high degree of measurement accuracy. A 10-s loading time was applied with an indenter load of 100 g. The indenter's impression area was determined from microphotographs by selecting the impression projection in automatic mode.

The study of porosity was carried out by the hydrostatic weighing method. Scales accurate to 0.01 g were used. To protect the specimen surfaces, they were coated with a layer of paraffin before immersion in distilled water. In calculating porosity, the density of the compact body was assumed to be equal to the density of the alloy in the cast state.

Alloying element distribution was investigated using X-ray spectral microanalysis (XRMS) conducted on a scanning electron microscope JSM-6360LA in mapping mode. The results were presented in the form of color maps, where areas with higher chemical element content corresponded to regions with more intense coloring.

X-ray diffractometric analysis was carried out on a HZG-4 diffractometer. Scanning was performed within the angle range of 10°–120° with a step size of 0.1°. Phase and chemical compound identification was accomplished through calculation-based methods using the "Match 3" software.

For the construction of specimens by the AFS-D method, consumable aluminum rods with a diameter of 12 mm were used. These rods were secured within a specialized spring mandrel mounted on a vertical milling machine (Figure 3).

The use of a spring mandrel allowed for the precise regulation and maintenance of the pressing force applied by the consumable rod's end against the substrate at a constant level. A steel bar was used as a substrate. The consumable rod was heated by a flow of heated air. The temperature within the plastic deformation zone of the rod was controlled with an accuracy of ±1°C using a noncontact pyrometer. Before processing, the substrate was heated to the operating temperature.

3. Results and Discussion

The process of constructing workpieces through friction stirring using the AFS-D method essentially consists of shearing a thin layer from the end of a rotating consumable rod that is pressed against a substrate (Figure 4).

In this case, as a first approximation, the processes occurring in the AFS-D method can be likened to those observed in specimens subjected to SPD by HPT [34]. The validity of using such an approach can be justified by the physical similarity of the occurring phenomena. This can be inferred from the consistent ratio of similar and characterizing values. The process of metal deformation at AFS-D and HPT can be described by similar differential equations as the basic conditions of unambiguity are fulfilled. These include the geometric shape and dimensions of the deformation zone, the similarity of physical (physical and chemical) material parameters, the initial conditions of the process (initial velocity, temperature, etc.), and the state of the system at its boundaries. Thus, it can be stated that the processes are geometrically and physically similar. This enables the application of similarity theory to investigate the AFS-D process concerning the development of properties and structure within a single thin layer of the specimen. The practical application of this conclusion lies in the examination of the formed material structure on small cylindrical specimens, obtained in the HPT process with different modes.

Microstructures of initial specimens (Figure 5(a)) and specimens after HPT with varying striker rotation speeds (Figures 5(b) and 5(c)) indicate the absence of macrofractures, such as pores or cracks, within the material. However, their density differs.

It was found that the density of the specimens in the initial state was 2558 kg/m^3, after HPT at 0.5 rpm–2775 kg/m^3 and at 1 rpm–2162 kg/m^3. Thus, the density of the specimens after deformation by HPT changed ambiguously. It decreased by 15% when subjected to torsion with higher speed and increased by 8% when subjected to torsion with lower speed (Figure 6).

The observed regularity can be explained by the appearance of strain gustiness coupled with material dehardening. In [35], the change in material's elastic limit is

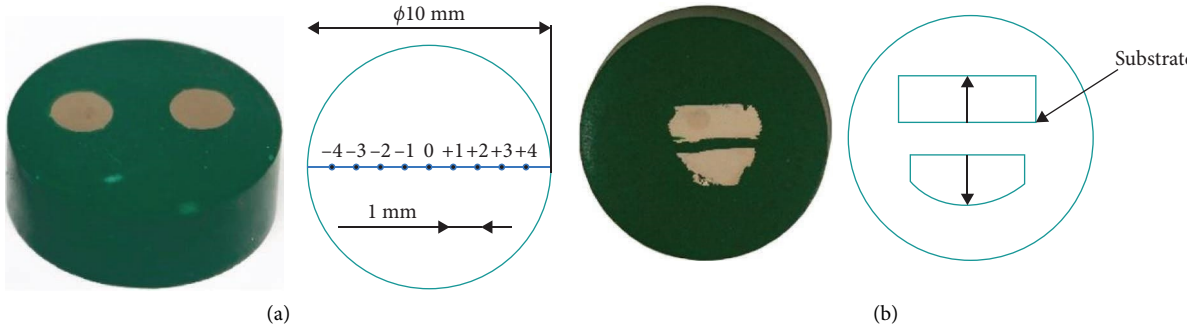

Figure 2: General view and scheme of microhardness measurement on specimen grinds after HPT (a) and AFS-D with cross-feed (b).

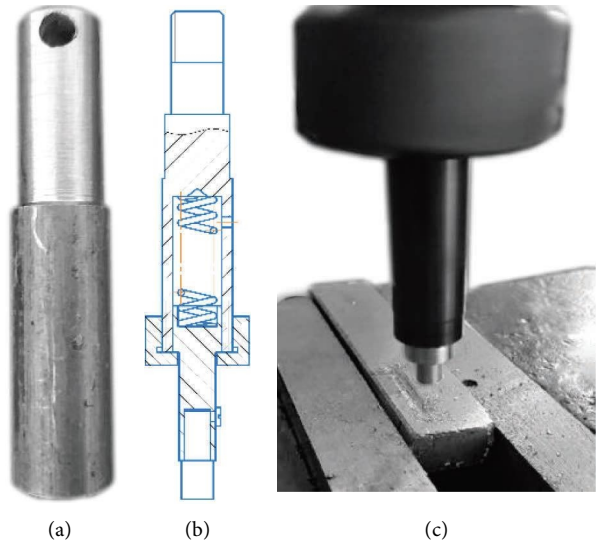

Figure 3: Consumable rod (a), spring mandrel (b), and the process of material layer applying (c).

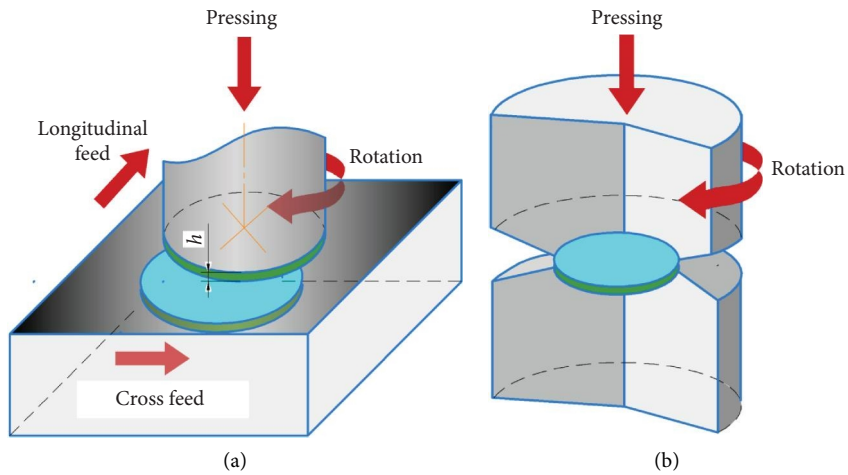

Figure 4: Motion kinematics during AFS-D (a) and HPT (b).

attributed to both hardening and loss of continuity, marked by the presence of submicroscopic cracks resulting from overpeening. Probably, the observed change in specimen density is associated with exceeding the rational degree of material deformation.

The analysis of microhardness distribution in initial specimens and specimens after HPT deformation revealed a number of basic regularities of strain hardening (Figure 7). After HPT, a radial hardening gradient was observed in the specimens. Microhardness values in the central part of both

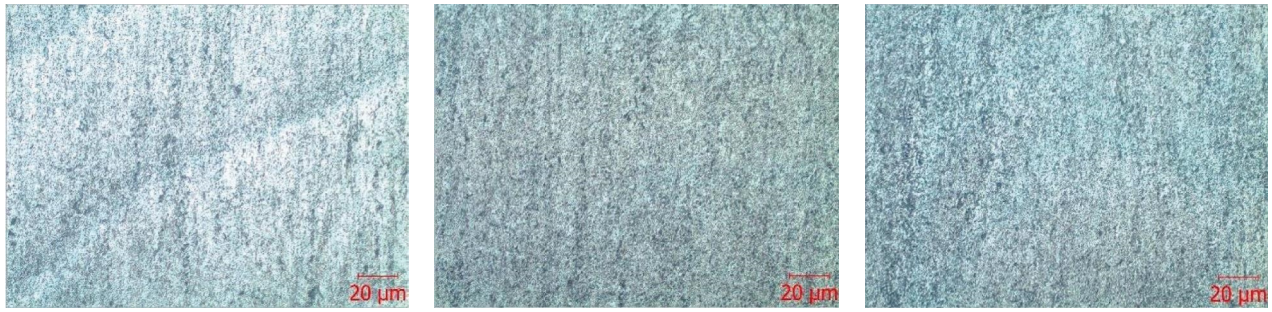

Figure 5: Microstructures of specimens in different states: (a) initial state (3D print); (b) after HPT at a speed of 0.5 rpm; (c) after HPT at a speed of 1 rpm.

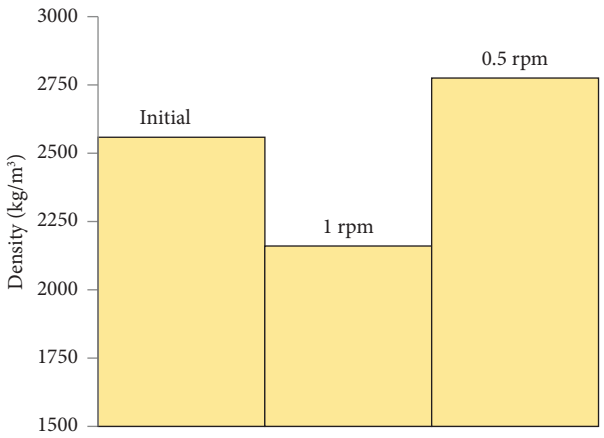

Figure 6: Change in density of specimens after HPT with different deformation speeds.

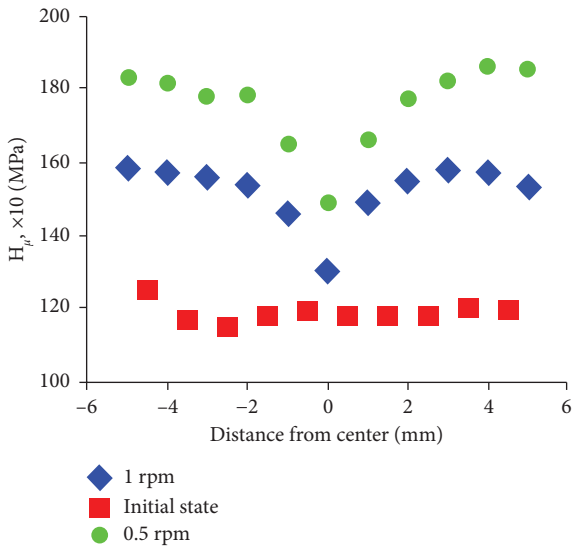

Figure 7: Microhardness distribution in the cross section of the specimens after HPT with different deformation speeds.

specimens were about 18% lower than in the periphery. The results of studies involving a similar alloy with comparable chemical composition indicate [36] that a uniform radial distribution of specimen microhardness is not achieved even at significantly higher degrees of deformation (10 turns).

From Figure 7, it is evident that the deformation speed significantly affects the microhardness values of the specimens. As the rotation speed of the strikers increased, the material's microhardness decreased. The hardening degree of the specimen peripheral part was 55% and 33% at rotation speeds of 0.5 rpm and 1 rpm, respectively. This observation might indicate concurrent hardening and softening processes during the treatment. Under similar experimental conditions, it is reasonable to suggest that specimen heating influences the hardening process. The increase in deformation speed is accompanied by an increase in its temperature and, probably, by dynamic recrystallization processes. The obtained results contrast with the study of Al 1050 alloy [37], where different deformation speeds (0.2 and 5 rpm) led to the same values of microhardness. This discrepancy could imply a substantial influence of the alloy grade on the patterns of strain hardening during the HPT process. Considering that material hardness indirectly reflects its strength characteristics, it becomes apparent that the deformation mode significantly impacts them. Consequently, to strengthen pre-eutectic silumin by intensive plastic deformation via HPT, it is essential to take into account not only the magnitude of pressure and strain but also the deformation speed.

Material properties are significantly influenced by the phase composition. It is known from the literature that the phase composition of various materials changes during HPT processes [38]. Considering that the accumulated strain during HPT can reach ~1.5 even on the specimen axis [39], its phase composition can also undergo changes.

The results of X-ray diffractometric analysis showed (Figure 8) that the position of diffraction peaks remains consistent between the initial specimen and those subjected to HPT, irrespective of the deformation mode. Traces of β''-phase (Mg_5Si_6) were detected in the specimens after annealing. Their absence in the deformed specimens suggests a potential decrease in their mass concentration to a level below the sensitivity threshold due to the mass transfer and mixing processes typical for SPD [40]. At the same time, a change in peak intensity and width was

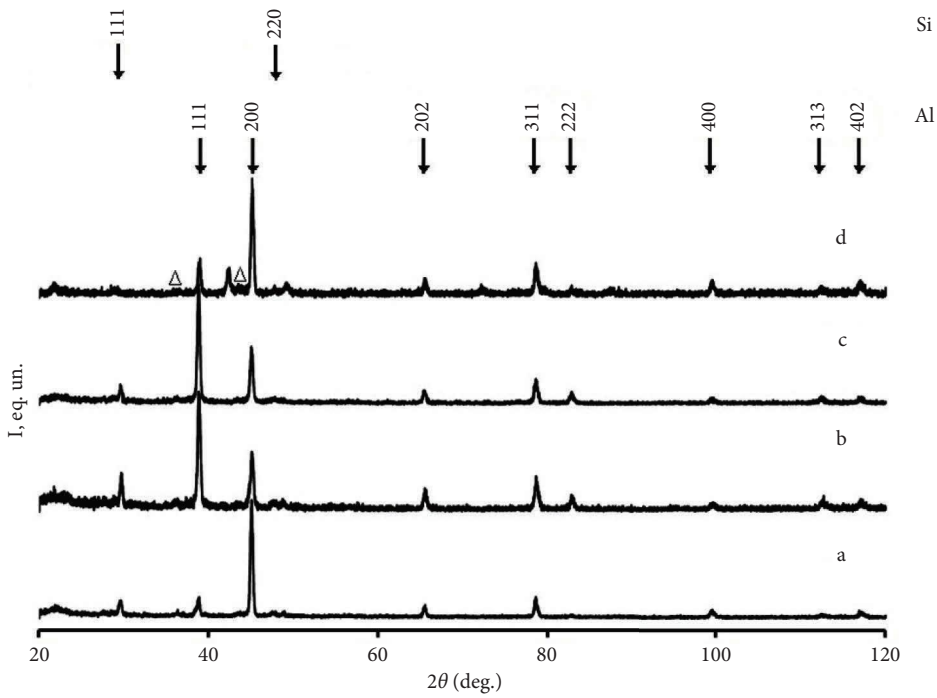

Figure 8: Diffractograms of specimens in different states: (a) initial state (3D print); (b) after HPT at a speed of 0.5 rpm; (c) after HPT at a speed of 1 rpm; (d) after annealing; Δ, traces of the β''-phase (Mg_5Si_6).

observed. The variation in intensity possibly indicates the development of a crystallographic texture, whereas changes in peak width may signify changes in crystallite size.

Quantitative analysis of the diffractograms indicates a fivefold, statistically significant decrease in the size of the coherent scattering region (CSR) (Table 1). At the same time, the size of the CSR did not depend on the deformation speed during the HPT process. It can also be stated that HPT did not lead to a change in the lattice parameter value.

The effect of vortex formation in a thin deformed layer of specimens, which is typical for metal deformation by simple shear [40], is accompanied by homogenization of alloying elements (Figure 9). The more homogeneous distribution of magnesium and silicon observed after HPT, coupled with grain refinement and the development of numerous high-angle grain boundaries, is also likely to contribute to strength improvement and reduction in scattering.

Specimens were built by the AFS-D method with longitudinal and cross-feed. With a favorable combination of temperature, force, and kinematic parameters of the process, high-strength bulk specimens were obtained in both cases (Figure 10).

As depicted in Figure 10, the process of workpiece construction involved the formation of thin concentric layers resulting from material flow under the thermomechanical action of the rotating tool and the preformed layer. At the tool exit location, the formation of two zones, conventionally termed the core zone and the peripheral zone, was observed.

The structure of the workpieces (Figures 11 and 12) was a set of layers, formed in the process of tool rotation. At the edges of the grind, noncontinuities and pores were observed. The formation of these defects in the peripheral zone is probably related to the peculiarities of the workpiece manufacturing technology. Their size and number can be regulated by selecting appropriate technological parameters. In the central zone, the microstructure of the AFS-D constructed workpieces in both longitudinal and cross directions (Figure 12) indicates the absence of microdefects in the form of noncontinuities typical of cast and powder workpieces (e.g., pores and flakes). In general, the macrostructure of the obtained specimens looks rather homogeneous, and the layering is not visualized.

The analysis of the cross-microgrind (Figures 11(b) and 12) perpendicular to the multilayer workpiece construction direction (Figures 11(b) and 12) allows us to visually distinguish discrete layers by insignificant microstructural differences. It can be explained by slight deviations in the thermal conditions of the layer's application related to the peculiarities in the heating of the tool working zone. However, there are no visible material defects at the boundaries of adjacent layers. This observation implies the potential to build dense workpieces with an unlimited number of layers.

The investigation of microhardness distribution in the cross and longitudinal sections of workpieces indicates regularity characteristic for the features of AFS-D method construction. Thus, in the cross direction of the workpieces constructed using the AFS-D method with cross-feed (Figures 10(b), 11(b), 12), the minimum microhardness value of 770 MPa. . .790 MPa corresponds to the upper layer formed at the stage of contact opening between the workpiece and the tool. The thickness of the layer with varying microhardness is about 2 mm. At the same time, the

Table 1: Quantitative characteristics of X-ray diffractometric analysis.

Specimen state, HPT deformation mode	Lattice parameter of aluminum-based solid solution a (Å)	CSR size D (nm)
3D print, initial	4.054	257 ± 30
1 rpm	4.054	56 ± 5
0.5 rpm	4.057	53 ± 6
After annealing	4.059	—

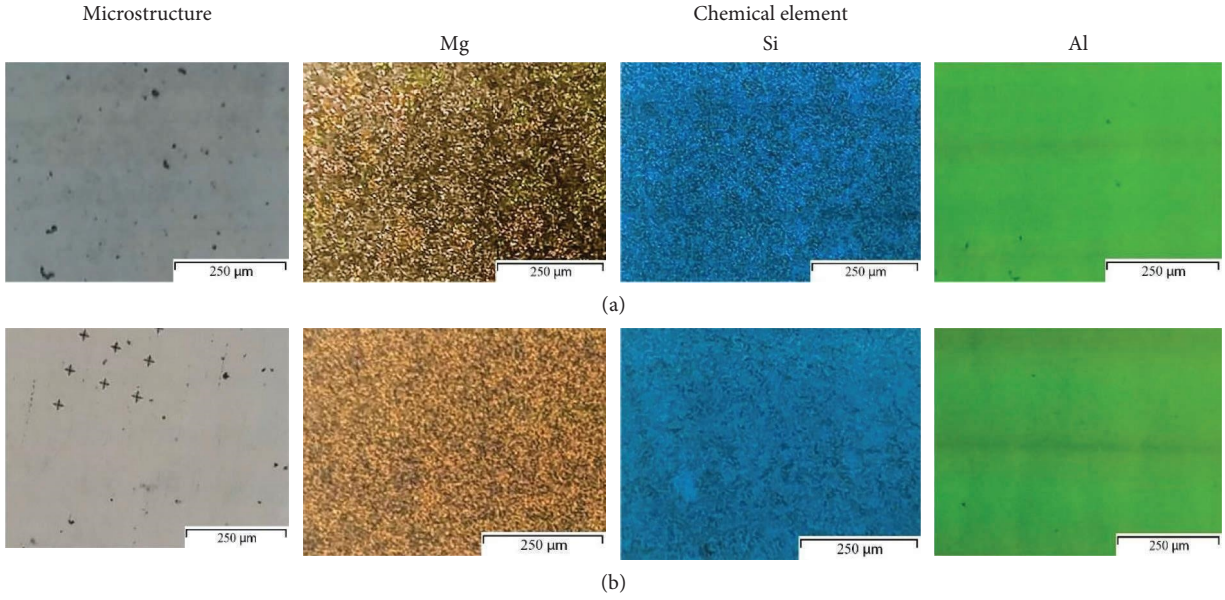

Figure 9: Electron micrographs and XRMS results in mapping mode for initial specimens (a) and after HPT (b).

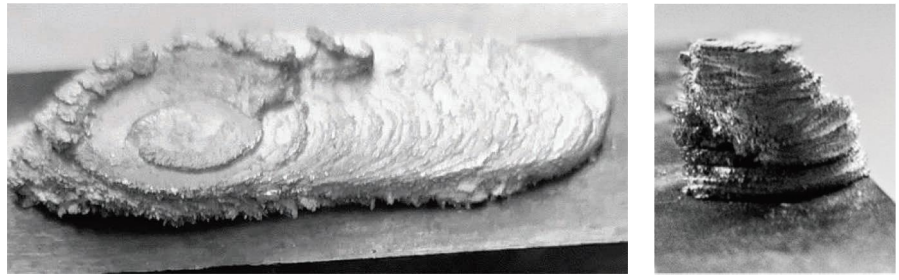

Figure 10: General view of three-layer specimens obtained by the AFS-D method with longitudinal (a) and cross-feed (b).

microhardness of the inner layers does not statistically differ and is in the range of 900 MPa. . .920 MPa for the investigated construction mode (Figure 13). This fact indicates the stability of the growth process and the mechanical properties of the obtained workpiece. The observed regularity of microhardness distribution in the upper part of the workpiece can be explained by the acceleration of tool movement in the axial direction for contact opening.

In the longitudinal direction of the workpiece constructed by AFS-D using the cross-feed method, the regularity of microhardness change has a similar characteristic to that of the HPT process (Figure 7). The lowest microhardness values are observed in the zone corresponding to the center of the consumed rod, ranging from 800 MPa to 820 MPa, whereas the highest values are in the peripheral areas, measuring 960 MPa–980 MPa (Figure 10(b)). The difference in microhardness amounts to roughly 20%. Similar to the deformation via the HPT method, this regularity is explained by the difference in the circumferential velocity of the tool. Considering the established dependence of microhardness on deformation speed in HPT-treated specimens, it can be assumed that an increase in the diameter of the consumable rod will also contribute to a heightened difference between the workpiece microhardness formed in its central and peripheral parts.

The observed regularity of microhardness distribution can be the cause of local differences in the physical and mechanical properties of AFS-D workpieces, as well as

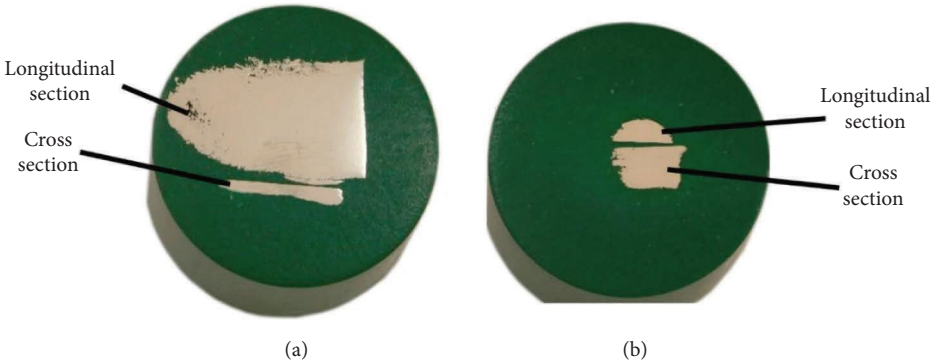

Figure 11: General view of longitudinal and cross sections of three-layer specimens obtained by the AFS-D method with longitudinal (a) and cross-feed (b).

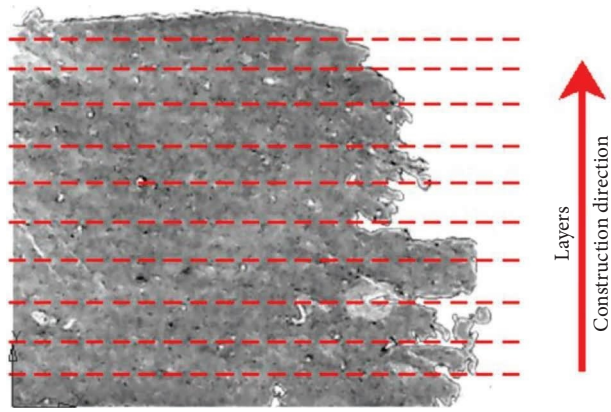

Figure 12: Macrostructure of the specimen cross section.

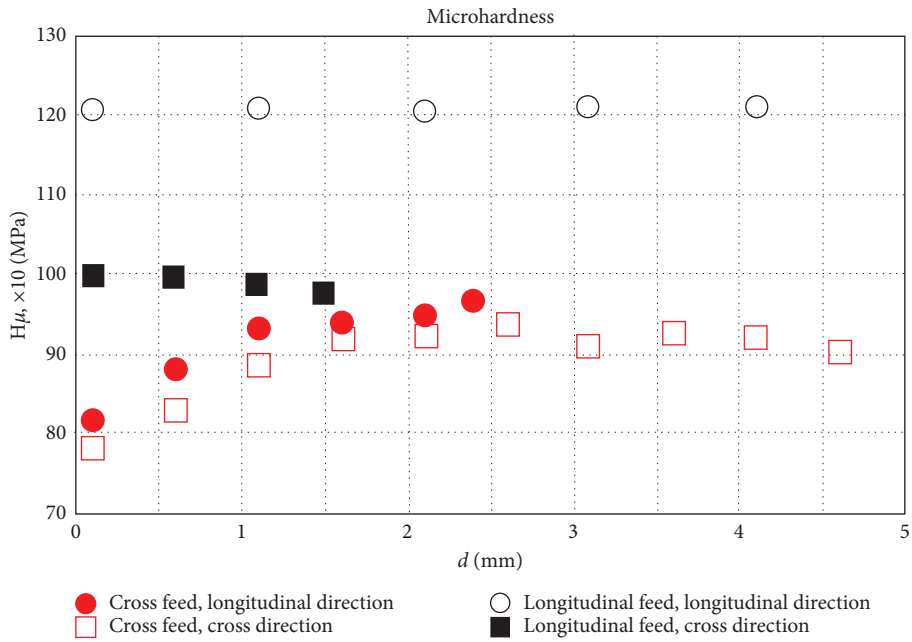

Figure 13: Microhardness distribution in cross and longitudinal directions of workpieces constructed by the AFS-D method.

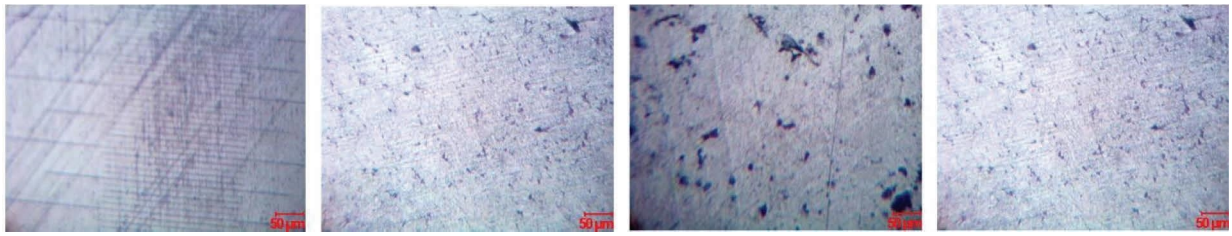

Figure 14: Microstructure of the initial consumable rod of D16 alloy.

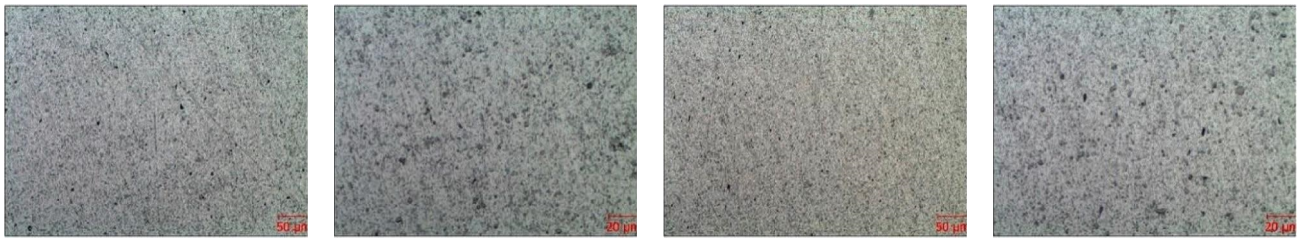

(a) (b) (c) (d)

Figure 15: Microstructure of specimens obtained by the AFS-D method with longitudinal feed: (a and b) cross direction; (c and d) longitudinal direction.

forming the internal architecture of the material. Controlling the construction strategy of individual layers opens up the possibility of changing the spatial orientation of workpiece regions with different properties. Their rational orientation with respect to the loads acting on the part during operation will increase the safety margin of the part with internal architecture in comparison with parts made of isotropic materials [41].

The microstructure of the initial consumable rod was typical for cast aluminum alloys, consisting of aluminum dendrites (light areas) and aluminum–silicon eutectics (dark areas) (Figure 14).

The investigation of the specimen microstructure obtained by the AFS-D method revealed its transformation compared to its initial state. It was found that the specimens had a homogeneous microstructure typical for deformable aluminum alloys. A uniform distribution of intermetallides on the grind surface was observed, likely owing to recrystallization of the alloy in the SPD process, resulting in the ultradispersed structure development. As can be seen from Figure 15(c), there is a tendency to form a "banded" structure.

Figure 16(d) shows a similar pattern of the certain directionality formation (in the form of "half-rings") in the microstructure due to the peculiarities of the tool motion.

During the research process, it was found that noncompliance with rational modes and construction conditions resulted in not only the appearance of defects in the workpieces but also the destruction of the consumable rod. The main types of its degradation were local material sticking (Figure 17(a)) and fluffing (Figure 17(b)). The appearance of such destruction led to the impossibility of further workpiece construction and the need to replace the consumable rod.

One of the key features of the AFS-D process is its ability to refine the grain structure due to SPD. However, it is important to note that the final grain size is likely to be influenced by the alloy composition. Generally, alloys with a higher content of alloying elements tend to exhibit larger final grain sizes compared to less alloyed materials when processed through AFS-D. This phenomenon has been observed in similar SPD processes.

It has been established that the application of AFS-D technology for the synthesis of aluminum alloy workpieces allows for obtaining a favorable microstructure typical for deformable alloys. The formation of an ultradispersed structure is observed, as in common SPD processes.

The AFS-D process offers a unique advantage in homogenizing existing alloys, which can significantly impact the microstructure and mechanical properties of the processed material. This method allows for a uniform distribution of alloying elements across the cross section of the product, positively influencing the overall mechanical properties. The peculiarities of the workpiece synthesis process enable us to consider the potential architectural formation of material properties according to the required part geometry.

Like any technology, AFS-D has advantages and disadvantages that may limit its application (Figure 18).

Based on the conducted experimental studies, a classifier of problems aimed at expanding the scope of this technology application in various industries has been developed (Figure 19).

The factors that condition and limit the introduction of AFS-D technology in industry, conventionally, to facilitate problem-solving, should be divided into several directions. Among them, the main ones are materials science, technology, and the direction related to the construction architecture.

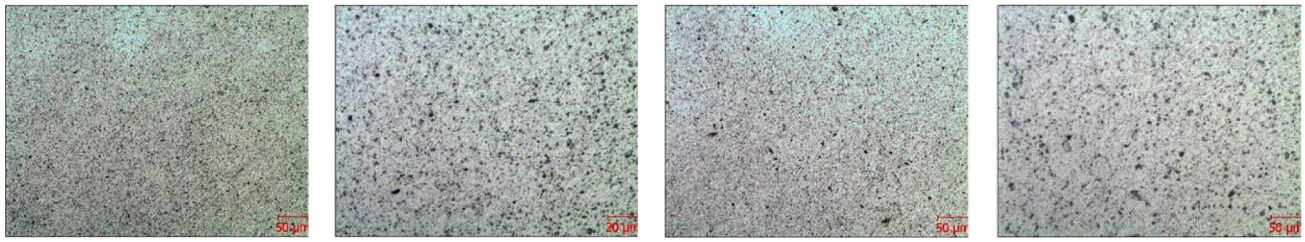

(a) (b) (c) (d)

Figure 16: Microstructure of specimens obtained by the AFS-D method with cross-feed: (a and b) cross direction; (c and d) longitudinal direction.

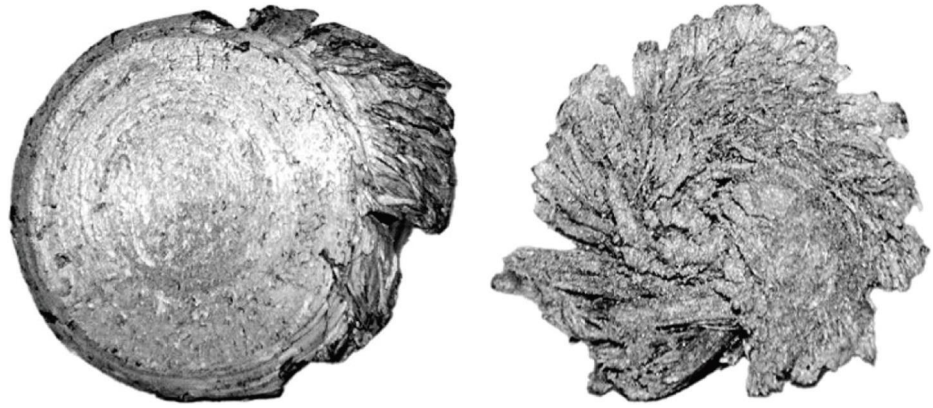

(a) (b)

Figure 17: General view of the consumable rod end surface destruction caused by material sticking (a) and fluffing (b).

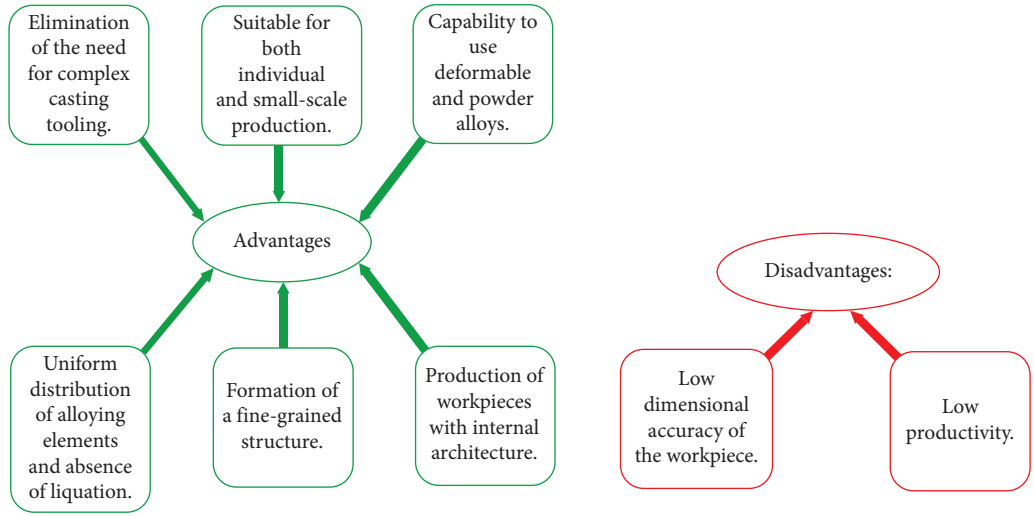

Figure 18: Advantages and disadvantages of AFS-D technology.

Addressing the outlined problems within each direction ensures the improvement of the finished part parameters. The particular issues to be resolved for part production using this technology vary based on the service purpose of the part. However, if all the problems specified in the classifier (Figure 18) are solved, the AFS-D technology will create serious

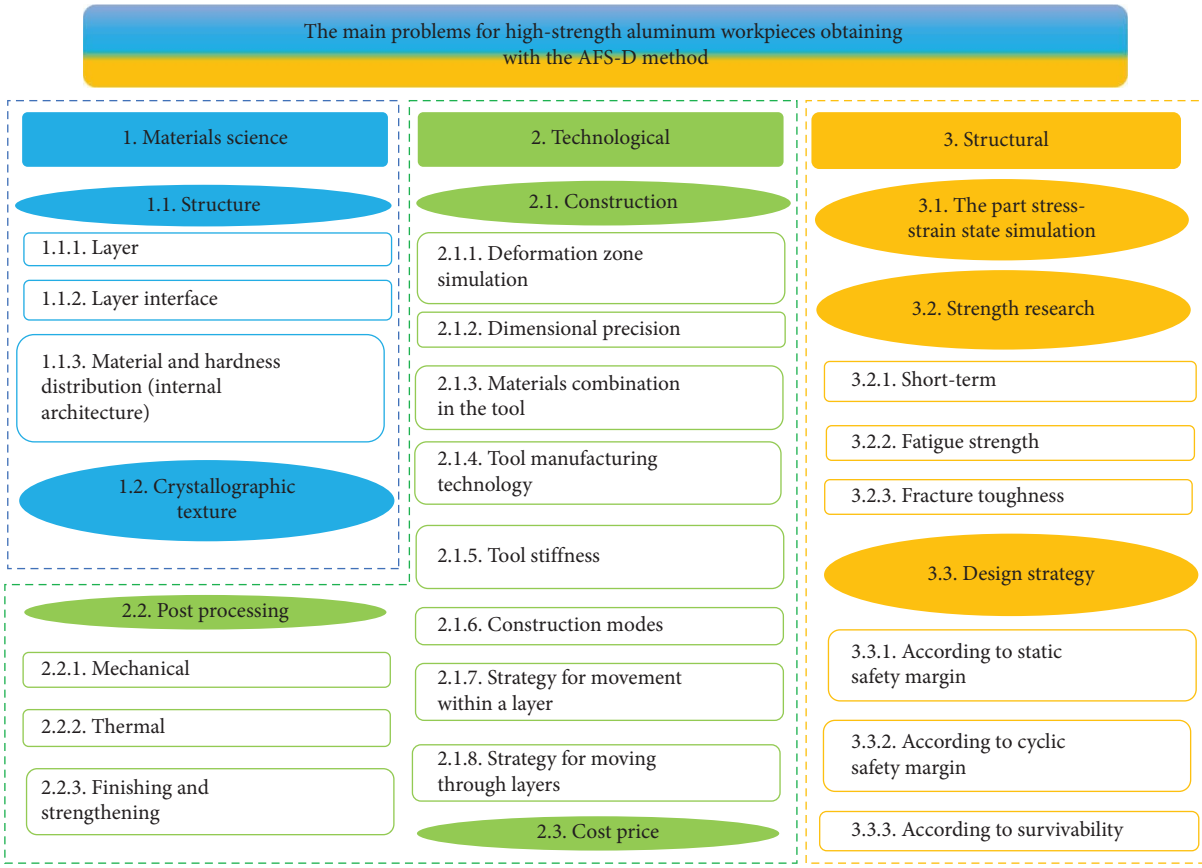

Figure 19: Problem classifier for introducing AFS-D in industry.

competition to traditional methods of part production, contributing to the improvement of their characteristics simultaneously with significant resource savings.

4. Conclusions

The results obtained demonstrate the potential of AFS-D for manufacturing high-quality aluminum alloy parts. The AFS-D process induces SPD analogous to HPT, enabling significant grain refinement. HPT testing of small specimens provides an expedient way to screen processing modes.

Specimens subjected to HPT exhibit different changes in density and microhardness depending on deformation speed: Processing with lower speed results in higher values. Microhardness distribution is typical for this process, revealing the difference of approximately 20% between center and periphery. The observed reduction in the size of the CSR, from 257 nm to 53...56 nm, indicates the significant crystallite fragmentation.

AFS-D specimens displayed homogeneous, fine-grained structures typical of deformable Al alloys with uniformly dispersed intermetallic phases, likely owing to dynamic recrystallization during processing. In the cross direction of workpieces created with cross-feed, the upper layer exhibited a minimum microhardness of 770...790 MPa during contact opening. This layer, with a thickness of about 2 mm, displayed varying microhardness. The microhardness of inner layers (900...920 MPa) remained statistically consistent, indicating stability in the growth process and mechanical properties. At the same time, in the longitudinal direction of these workpieces, the microhardness change pattern closely resembles that of the HPT process.

Thus, the obtained results suggest that in selecting AFS-D process parameters, considerations should extend beyond pressure and strain values to also encompass deformation speed. Failing to follow optimal processing conditions risks defects and tool damage. To obtain workpieces of complex configuration, it is promising to use multi-axis machining centers that allow changing tool blocks with fixed consumable rods in automatic mode, industrial implementation, and qualification trials.

In summary, AFS-D is an efficient technique for manufacturing enhanced Al alloy parts versus conventional methods. The ultrafine grains and lack of casting flaws demonstrate advantages over other additive approaches reliant on melting. By inducing intense deformation analogous to SPD, AFS-D generates wrought-like structures in as-deposited parts with properties superior to casting. This makes AFS-D an appealing production route for critical aerospace and defense parts.

The prospect of further research is to study the features of structure and mechanical and physical properties of workpieces processed by HPT with different modes. To address challenges associated with the AFS-D process industrial scaling, further research and development are

planned, focusing on process parameter optimization, real-time monitoring and control systems, improved tool designs, postprocessing methods, simulation, and modeling for defect prevention. Successfully overcoming these hurdles will unlock AFS-D's potential for producing high-quality components, particularly in industries demanding high-performance, lightweight parts such as aerospace and automotive sectors.

Data Availability Statement

The data that support the findings of this study are available from the corresponding author upon reasonable request.

Conflicts of Interest

The authors declare no conflicts of interest.

Funding

No funding was received for this research.

References

[1] G. R. Kumar, M. Sathishkumar, M. Vignesh, et al., "Metal Additive Manufacturing of Commercial Aerospace Components–A Comprehensive Review," *Proceedings of the Institution of Mechanical Engineers-Part E: Journal of Process Mechanical Engineering* 237, no. 2 (2023): 441–454, https://doi.org/10.1177/09544089221104070.

[2] Standardization Roadmap for Additive Manufacturing, "America Makes and ANSI Additive Manufacturing Standardization Collaborative (AMSC)," (2018): https://www.ansi.org/standards-coordination/collaboratives-activities/additive-manufacturing-collaborative.

[3] R. Fu, Y. Guo, Y. Cui, J. Wang, H. Lei, and C. Liu, "Large-Size Ultra-High Strength-Plasticity Aluminum Alloys Fabricated by Wire Arc Additive Manufacturing via Added Nanoparticles," *Materials Science and Engineering A* 864, no. 2 (2023): 144582, https://doi.org/10.1016/j.msea.2023.144582.

[4] R. Z. Valiev, "Nanostructural Design of Superstrong Metallic Materials by Severe Plastic Deformation Processing," *Microstructures* 3, no. 1 (2023): 2023004, https://doi.org/10.20517/microstructures.2022.25.

[5] E. M. Sefene, "State-of-the-Art of Selective Laser Melting Process: A Comprehensive Review," *Journal of Manufacturing Systems* 63 (2022): 250–274, https://doi.org/10.1016/j.jmsy.2022.04.002.

[6] K. Wang, W. Liu, Y. Hong, et al., "An Overview of Technological Parameter Optimization in the Case of Laser Cladding," *Coatings* 13, no. 3 (2023): 496, https://doi.org/10.3390/coatings13030496.

[7] D. Tkach, D. Pavlenko, Y. Dvirnyk, O. Pedash, and O. Tarasov, "The Main Defects and Ways to Improve the Quality of Layer-by-Layer Sintered Gas Turbine Parts," *Smart Technologies in Urban Engineering* (2023): 536, Springer, Berlin, Germany, https://doi.org/10.1007/978-3-031-20141-7_48.

[8] J. J. S. Dilip, G. J. Ram, and B. E. Stucker, "Additive Manufacturing With Friction Welding and Friction Deposition Processes," *International Journal of Rapid Manufacturing* 3, no. 1 (2012): 56–69, https://doi.org/10.1504/ijrapidm.2012.046574.

[9] M. Vaezi, P. Drescher, and H. Seitz, "Beamless Metal Additive Manufacturing," *Materials* 13, no. 4 (2020): 922, https://doi.org/10.3390/ma13040922.

[10] W. V. Twelves, W. Lin, and D. G. Alexander, "Solid State Additive Manufacturing System," (2009): US20090200275A1.

[11] S. Palanivel and R. S. Mishra, "Building Without Melting: A Short Review of Friction-Based Additive Manufacturing Techniques," *International Journal of Additive and Subtractive Materials Manufacturing* 1, no. 1 (2017): 82–103, https://doi.org/10.1504/ijasmm.2017.082991.

[12] H. Z. Yu, M. E. Jones, G. W. Brady, et al., "Non-Beam-Based Metal Additive Manufacturing Enabled by Additive Friction Stir Deposition," *Scripta Materialia* 153 (2018): 122–130, https://doi.org/10.1016/j.scriptamat.2018.03.025.

[13] M. K. Kulekci, U. Esme, and B. Buldum, "Critical Analysis of Friction Stir-Based Manufacturing Processes," *The International Journal of Advanced Manufacturing Technology* 85, no. 5-8 (2016): 1687–1712, https://doi.org/10.1007/s00170-015-8071-5.

[14] J. J. S. Dilip, S. Babu, S. V. Rajan, K. H. Rafi, G. J. Ram, and B. E. Stucker, "Use of Friction Surfacing for Additive Manufacturing," *Materials and Manufacturing Processes* 28, no. 2 (2013): 189–194, https://doi.org/10.1080/10426914.2012.677912.

[15] M. Li, "Development and Prospect of Friction Surfacing Technology," in *Proceedings of the 5th International Symposium on Knowledge Acquisition and Modeling*, 244–246, Atlantis Press, London, UK, June 2015, https://doi.org/10.2991/kam-15.2015.67.

[16] R. G. S. Nixon, B. S. Mohanty, and G. B. Bhaskar, "Effect of Process Parameters on Physical Measurements of AISI316 Stainless Steel Coating on EN24 in Friction Surfacing," *Materials and Manufacturing Processes* 33, no. 7 (2017): 778–785, https://doi.org/10.1080/10426914.2017.1388524.

[17] Z. J. Tan, P. Ge, and Z. Zhang, "Finite Element Simulation of Friction Stir Additive Manufacturing," in *Proceedings of the 8th International Conference on Computational Methods*, Guilin, China, July 2017.

[18] Z. Zhang, Z.-J. Tan, J.-Y. Li, Y.-F. Zu, and J.-J. Sha, "Integrated Modeling of Process-Microstructure-Property Relations in Friction Stir Additive Manufacturing," *Acta Metallurgica Sinica* 33, no. 1 (2020): 75–87, https://doi.org/10.1007/s40195-019-00945-9.

[19] X.-K. Wang, L. Xing, W.-P. Xu, C.-P. Huang, and F.-C. Liu, "Influence of Process Parameters on Formation of Friction Stir Additive Manufacturing on Aluminum Alloy," *Cailiao Gongcheng/Journal of Materials Engineering* 43, no. 5 (2015): 8–12.

[20] J. Blindheim, T. Welo, and M. Steinert, "First Demonstration of a New Additive Manufacturing Process Based on Metal Extrusion and Solid-State Bonding," *The International Journal of Advanced Manufacturing Technology* 105, no. 5-6 (2019): 2523–2530, https://doi.org/10.1007/s00170-019-04385-8.

[21] J. C. Galvis, P. H. F. Oliveira, J. D. P. Martins, and A. L. M. Carvalho, "Assessment of Process Parameters by Friction Surfacing on the Double Layer Deposition," *Materials Research* 21, no. 3 (2018): 1–11, https://doi.org/10.1590/1980-5373-mr-2018-0051.

[22] H. Tokisue, K. Katoh, T. Asahina, and T. Ushiyama, "Structures and Mechanical Properties of Multilayer Friction Surfaced Aluminum Alloys," *Report of the Research Institute of Industrial Technology* 78 (2005): 1–13.

[23] X.-R. Fu, L. Xing, C.-P. Huang, F.-C. Liu, and L.-M. Ke, "Microstructure of 2024 Aluminum Alloy by Stationary

Shoulder Friction Stir Additive Manufacturing," *Chinese Journal of Nonferrous Metals* 29 (2019): 1591.

[24] P. S. Michael, *Additive Friction Stir Manufacturing of 7055 Aluminum Alloy: Senior Honors Theses* (New Orleans, LA, University of New Orleans, 2016).

[25] Z. Kallien, L. Rath, A. Roos, and B. Klusemann, "Experimentally Established Correlation of Friction Surfacing Process Temperature and Deposit Geometry," *Surface and Coatings Technology* 397 (2020): 126040, https://doi.org/10.1016/j.surfcoat.2020.126040.

[26] S. Klingensmith, J. N. Dupont, and A. R. Marder, "Microstructural Characterization of a Double-Sided Friction Stir Weld on a Superaustenitic Stainless Steel," *Welding Journal* 5 (2005): 77–85.

[27] W. J. Arbegast, "Friction Stir Welding. After a Decade of Development," *Welding Journal* 85, no. 3 (2006): 28–35.

[28] J. P. Schultz and K. D. Creehan, "Fabrication Tools for Exerting Normal Forces on Feedstock," (2017): US9643279B2.

[29] J. P. Schultz and K. D. Creehan, "Fabrication Tools for Exerting Normal Forces on Feedstock," (2015): US9205578B2.

[30] J. P. Schultz and K. D. Creehan, "Friction Fabrication Tools," (2014): US8632850B2.

[31] J. P. Schultz and K. D. Creehan, "System for Continuous Feeding of Filler Material for Friction Stir Welding, Processing and Fabrication," (2014): US8875976B2.

[32] J. P. Schultz and K. D. Creehan, "Self-Reacting Friction Stir Welding Tool With the Ability to Add Filler Material," (2013): US8397974B2.

[33] H. Chen, X. Meng, J. Chen, et al., "Wire-Based Friction Stir Additive Manufacturing," *Additive Manufacturing* 70 (2023): 103557, https://doi.org/10.1016/j.addma.2023.103557.

[34] Y. Beygelzimer, Y. Estrin, O. Davydenko, and R. Kulagin, "Gripping Prospective of Non-Shear Flows Under High-Pressure Torsion," *Materials* 16, no. 2 (2023): 823, https://doi.org/10.3390/ma16020823.

[35] D. V. Pavlenko, S. V. Loskutov, V. K. Yatsenko, and N. V. Gonchar, "Structural Changes in the Surface Layers of an EK79-ID Alloy Upon Hardening Treatments," *Technical Physics Letters* 29, no. 4 (2003): 345–346, https://doi.org/10.1134/1.1573312.

[36] S. M. Yusuf, M. Hoegden, and N. Gao, "Effect of Sample Orientation on the Microstructure and Microhardness of Additively Manufactured AlSi10Mg Processed by High-Pressure Torsion," *The International Journal of Advanced Manufacturing Technology* 106, no. 9-10 (2020): 4321–4337, https://doi.org/10.1007/s00170-019-04817-5.

[37] Y. Todaka, M. Umemoto, A. Yamazaki, J. Sasaki, and K. Tsuchiya, "Influence of High-Pressure Torsion Straining Conditions on Microstructure Evolution in Commercial Purity Aluminum," *Materials Transactions* 49, no. 1 (2008): 7–14, https://doi.org/10.2320/matertrans.me200713.

[38] L. Yuan, X. Zeng, X. Zhao, Y. Xie, J. Gandra, and D. Guan, "Microstructure Evolution and Tensile Behaviour of Fine-Grained 6082 Al Wire With High Ultimate Strength and High Work Hardening by Friction Stir Extrusion of Bulk Al Sheet," *Materials Science and Engineering A* 864 (2023): 144589, https://doi.org/10.1016/j.msea.2023.144589.

[39] D. Nugmanov, R. Kulagin, O. Perroud, M. Mail, H. Hahn, and Y. Ivanisenko, "Equivalent Strain Distribution at High Pressure Torsion Extrusion of Pure Copper: Finite Element Modeling and Experimental Validation," *Journal of Materials Processing Technology* 315, no. 11 (2023): 117932, https://doi.org/10.1016/j.jmatprotec.2023.117932.

[40] D. V. Pavlenko and Y. E. Beygel'zimer, "Theory and Technology of Forming Process: Vortices in Noncompact Blanks During Twist Extrusion," *Powder Metallurgy and Metal Ceramics (Translation of Poroshkovaya Metallurgiya (Kiev))* 54, no. 9-10 (2016): 517–524, https://doi.org/10.1007/s11106-016-9744-9.

[41] Y. Beihelzimer, R. Kulahin, and Y. Estrin, "Severe Plastic Deformation as a Way to Produce Architectured Materials, Architectured Materials," in *Nature and Engineering* (2019): 231–255, Springer, Berlin, Germany, https://doi.org/10.1007/978-3-030-11942-3_8.